

PAPER

Improved decentralized GNSS/SINS/odometer fusion system for land vehicle navigation applications

To cite this article: Mengxue Mu and Long Zhao 2023 *Meas. Sci. Technol.* **34** 035117

View the [article online](#) for updates and enhancements.

You may also like

- [Backtracking scheme for single-point self-calibration and rapid in-motion alignment with application to a position and azimuth determining system](#)
Jiazhen Lu, Shufang Liang and Yanqiang Yang
- [Achieving traceability to UTC through GNSS measurements](#)
P Defraigne, J Achkar, M J Coleman et al.
- [Universal adic approximation, invariant measures and scaled entropy](#)
A. M. Vershik and P. B. Zatitskii



ECS Toyota Young Investigator Fellowship

For young professionals and scholars pursuing research in batteries, fuel cells and hydrogen, and future sustainable technologies.

At least one \$50,000 fellowship is available annually.
More than \$1.4 million awarded since 2015!

 Application deadline: January 31, 2023

Learn more. Apply today!

The advertisement banner features a dark background with a glowing globe and various scientific icons. The ECS and TOYOTA logos are prominently displayed in the top right corner.

Improved decentralized GNSS/SINS/odometer fusion system for land vehicle navigation applications

Mengxue Mu^{1,2} and Long Zhao^{1,2,3,*} 

¹ School of Automation Science and Electrical Engineering, Beihang University, Beijing 100191, People's Republic of China

² Digital Navigation Center, Beihang University, Beijing 100191, People's Republic of China

³ Science and Technology on Aircraft Control Laboratory, Beihang University, Beijing 100191, People's Republic of China

E-mail: buaa_dnc@buaa.edu.cn

Received 22 September 2022, revised 23 November 2022

Accepted for publication 7 December 2022

Published 21 December 2022



Abstract

Due to low cost and complementary performance advantages, global navigation satellite system (GNSS)/ strapdown inertial navigation system (SINS) integrated systems have established themselves in certain areas of land vehicle navigation. However, this integrated system cannot maintain reliable positioning solutions in challenging environments due to the inherent fragility of GNSS signals and time accumulated errors of a stand-alone SINS. To address this challenge, a multi-source information fusion system based on the decentralized system architecture and sequential Kalman filter for a land vehicle is proposed, which can fuse information from an odometer and motion aided constraints selectively and adaptively in different driving environments. Moreover, a comprehensive calibration and compensation strategy is designed to enhance the information fusion. On the one hand, a real-time calibration algorithm is designed to estimate the time-varying odometer scale factor and the misalignment between the inertial measurement unit (IMU) and vehicle body frame when GNSS signals are available. On the other hand, the forward velocity error caused by the lever arm, and the non-zero lateral velocity generated by the turning maneuver are compensated by the introduced velocity compensation method. A real car experiment in urban areas is carried out to illustrate the effectiveness of the proposed system. It shows that the proposed decentralized GNSS/SINS/odometer fusion system can maintain an average horizontal positioning root mean square error (RMSE) of 1-meter level when GNSS signals are cut off about 1-2 min. In addition, compared with the traditional centralized fusion structure, the proposed decentralized fusion structure can mitigate the horizontal positioning RMSE of the whole trajectory from 2.95 m to 0.59 m, which verifies that it can obtain better performance for the application of low-cost sensors in complex GNSS environments.

Keywords: GNSS/SINS/odometer fusion system, odometer scale factor, IMU misalignment, lever arm, sequential Kalman filter

(Some figures may appear in colour only in the online journal)

* Author to whom any correspondence should be addressed.

1. Introduction

Global navigation satellite system (GNSS) integrated with the strapdown inertial navigation system (SINS) plays an important role in the land vehicle positioning due to its low cost, wide availability and complementary properties [1–4]. However, the integrated system is often degraded into a single SINS in signal interference and obstructed environments such as urban canyons and tunnels, which is impossible to provide the desired positioning service [5]. Adding additional positioning and navigation sources, namely multi-source information fusion, is generally adopted to constrain the SINS errors and improve the system quality in a poor GNSS environment [6, 7]. The commonly used information sources can be categorized into real observations and virtual observations. The former is provided by physical sensors, such as odometers, steering encoders, barometers, and cameras [8–11], and the latter is offered by motion aided constraints (MACs) [12, 13] or various neural networks [14, 15].

Among the many additional information sources, odometers and MACs are the most popular ones for the reason of lower computational complexity and no more extra sensors need to be mounted in automobiles [16, 17]. An odometer produces a continual impulse count with high frequency, which can be converted to the vehicle's forward velocity by multiplying a scale factor [18, 19]. Thus, the rapidly increasing positioning errors caused by drifts of a stand-alone SINS can be suppressed by the integration of an odometer. MACs can provide virtual velocity observations according to the motion and driving situation of the vehicle to prohibit the divergence of SINS errors. As one of MACs, non-holonomic constraint (NHC) assumes that the lateral and vertical velocity component should be close to zero when the vehicle is moving on a planar road surface without slides and jumps [8]. GNSS/SINS integrated system can benefit from the combination of the odometer and NHC due to the additional 3D velocity constraint information in a GNSS-denied environment.

To enhance the positioning performance implemented by the fusion of the odometer and MACs, the following four issues should be addressed. First, the odometer scale factor is not a nominal constant value and it drifts with the change of load and tire pressure. Second, the odometer measures the velocity in the vehicle body frame (VBF) rather than the inertial sensor frame. Therefore, the misalignment between the inertial measurement unit (IMU) sensor frame and VBF makes the velocity converted from the VBF to the navigation frame inaccurate, which is the same problem NHC may face [20]. Third, the lever arm between the IMU origin and odometer origin generates velocity measurement errors during turning maneuvers [21]. Last but not least, the assistance of NHC may be unavailable due to the non-zero lateral velocity component during fast steering maneuvers of the land vehicle [22]. In the previous research, the calibration of the scale factor, IMU misalignment and lever arm is simultaneously conducted with the estimation of SINS error states through a centralized Kalman filter on the basis of a 21-dimensional error state vector and a velocity error observation [23]. From the observability analysis of error states, the performance of the

proposed method largely depends on the measurement accuracy of the gyroscope, which is more suitable for high-precision IMU rather than low-cost micro-electromechanical systems (MEMS)-based IMU [19]. Besides, the coefficient of the lever arm error state, defined as the angular velocity of IMU relative to the earth, may be close to zero and remain constant when the land vehicle conforms to NHC and performs no turning maneuvers. Thus, whether the calibration of the lever arm can be realized or not is decided by the maneuvers of the land vehicle and the measurement accuracy of the gyroscope. Chen *et al* [16] addressed the accurate estimation of IMU misalignment by fusing the GNSS/SINS integrated position with a dead reckoning (DR) through a straight forward Kalman filter, where the DR is realized by the GNSS/SINS integrated attitude and traveled distance. This research reported that compared with the existing velocity-level observation-based method, the position-level observation might achieve better accuracy. However, the velocity compensation of the lever arm was not elaborated, especially when the odometer was mounted on the steering wheel instead of non-steering wheel. Moreover, the lateral velocity is mostly ignored in the existing literature when applying NHC during turning maneuvers. Gao and Zhao [22] utilized the context awareness technology to distinguish the vehicle's motion behavior, and only applied NHC when a rectilinear motion was detected. However, it is difficult to maintain a rigorous rectilinear motion in the real road environment, and the existence of lateral velocity may lead to residual observation errors in the application of NHC. Therefore, a comprehensive calibration and compensation strategy is necessary to improve the fusion performance when the odometer is integrated with a low-cost MEMS-based IMU.

Motivated by the above literature, an improved decentralized GNSS/SINS/odometer fusion system with a comprehensive calibration and compensation strategy for land vehicle is studied here to improve the positioning performance in GNSS-denied environments, which can selectively work in two modes: GNSS/SINS fusion mode and SINS/odometer fusion mode. The GNSS/SINS fusion mode will provide positioning service and simultaneously calibrate the odometer scale factor and IMU misalignment when GNSS signals are available. Whereas, when GNSS signals are poor or unavailable, the SINS/odometer fusion mode will be switched on to offer a positioning solution and the calibrated parameters are utilized to improve positioning accuracy. To facilitate the fusion procedure and fault detection and isolation, a decentralized fusion system architecture is designed. In addition, a sequential Kalman filter is adopted to improve the computing efficiency, which can avoid the calculation of high-order inverse matrix by processing the observation one by one [24, 25]. The main contributions are summarized as follows.

- A real time calibration algorithm for the low-cost GNSS/SINS/odometer fusion system is proposed based on the establishment of an odometer position error propagation equation. It can achieve more accurate estimation of the odometer scale factor and the IMU misalignment compared

with the traditional calibration method using the velocity-level observation.

- A velocity compensation model according to the Ackermann steering geometry is provided to achieve a more accurate odometer velocity observation. It can not only eliminate the forward velocity error caused by the unobservable lever arm, but also mitigate the always neglected lateral velocity error when applying the NHC.
- A decentralized fusion system architecture combined with the sequential Kalman filter is designed to facilitate the fusion of multi-source information. As a result, a better positioning performance is obtained no matter GNSS signals are available or not compared with the centralized structure.

The odometer position error propagation equation and the real time calibration algorithm are first introduced, followed by the velocity compensation model. Then, the designed decentralized GNSS/SINS/odometer fusion system and sequential Kalman filter are elaborated. Finally, the results of a real car experiment and detailed analysis are presented.

2. Real time calibration algorithm

DR algorithm and the establishment of odometer position error propagation equation are presented in this section, followed by the calibration algorithm, which can estimate the odometer scale factor error and IMU misalignment error in real time.

The coordinate frame used here are the VBF (b -frame) with three axes pointing to the front, right, and down (FRD) direction, the inertial sensor frame (m -frame) with three axes pointing to the FRD direction, the inertial frame (i -frame), the navigation frame (n -frame), and the earth-centered earth-fixed frame (e -frame). The definition, transform matrices and illustration of these coordinate frames can be found in [26].

2.1. Dead reckoning

An odometer or a wheel encoder can be installed on any wheel center or any axle center of the vehicle. It is generally assumed that an odometer measures the forward velocity of the vehicle, and it can be combined with NHC to provide a 3D velocity measurement. According to the assumption of NHC, the lateral and vertical velocity components of the vehicle are close to zero. Thus, the measurement model is given by

$$\mathbf{V}_O^b = [V_O \ 0 \ 0]^T = [k_O N_O \ 0 \ 0]^T \quad (1)$$

where \mathbf{V}_O^b denotes the velocity expressed in b -frame with the subscript means that it is calculated by an odometer, V_O represents the measured forward velocity, k_O denotes the odometer scale factor, and N_O denotes the impulse count. The theoretical velocity expressed in n -frame is obtained as

$$\mathbf{V}_O^n = \mathbf{C}_b^n \mathbf{V}_O^b = \mathbf{C}_m^n \mathbf{C}_b^m [V_O \ 0 \ 0]^T \quad (2)$$

where \mathbf{C}_b^n is the direction cosine matrix consisting of the vehicle attitude Φ , \mathbf{C}_m^n is the IMU attitude matrix calculated by SINS update, and \mathbf{C}_b^m is the IMU misalignment matrix made

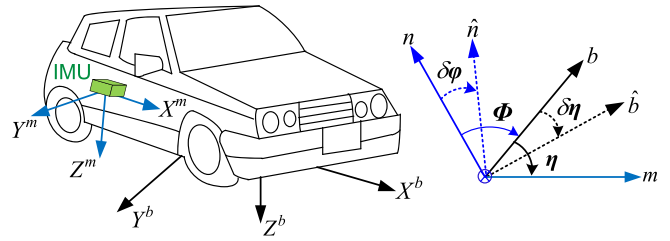


Figure 1. Relationship between the vehicle attitude and misalignment angle.

up of the misalignment angle η . The relationship between the vehicle attitude and misalignment angle is illustrated in figure 1, where \hat{n} -frame is the calculated navigation frame contaminated by the attitude error $\delta\varphi$, and \hat{b} -frame is the calculated VBF contaminated by the misalignment error $\delta\eta$. When IMU is well aligned and mounted, m -frame should coincide with b -frame and \mathbf{C}_b^m is an identity matrix.

The position provided by the odometer is deduced from the position differential equation. Let $L_O(k-1)$, $\lambda_O(k-1)$, and $H_O(k-1)$ represent the longitude, latitude and height provided by the odometer at epoch $k-1$, thus the position at k epoch is updated by [14]

$$\mathbf{P}_{O,k}^n = \begin{bmatrix} L_{O,k-1} \\ \lambda_{O,k-1} \\ H_{O,k-1} \end{bmatrix} + \begin{bmatrix} \frac{V_{ON,k}^n}{R_{M,k-1} + H_{O,k-1}} \\ \frac{V_{OE,k}^n}{(R_{N,k-1} + H_{O,k-1}) \cos L_{O,k-1}} \\ -V_{OD,k}^n \end{bmatrix} \Delta t \quad (3)$$

where $\mathbf{P}_O^n(k) = [L_{O,k} \ \lambda_{O,k} \ H_{O,k}]^T$ denotes the position vector calculated by an odometer and expressed in n -frame at k epoch, Δt is the sample interval, R_M is the meridian radius, R_N is the prime vertical radius, and V_{ON}^n , V_{OE}^n , and V_{OD}^n denotes the velocity component of \mathbf{V}_O^n in the north, east, and down direction, respectively.

2.2. Position error propagation equation

The scale factor of the odometer always varies with the variation of wheel diameter, which may be caused by the change of temperature, tire pressure, load and land surface conditions. Let δk_O be the odometer scale factor error, then the velocity measurement in (1) is calculated as

$$\hat{\mathbf{V}}_O^b = [(k_O + \delta k_O) N_O \ 0 \ 0]^T = [(1 + \delta \bar{k}_O) V_O \ 0 \ 0]^T \quad (4)$$

where $\delta \bar{k}_O = \delta k_O / k_O$ denotes the normalized odometer scale factor error.

According to figure 1, the converted velocity in (2) may contain errors due to the IMU misalignment error $\delta\eta$ and attitude error $\delta\varphi$ in the direction cosine matrix \mathbf{C}_b^n . During the calibration of IMU misalignment, the influence caused by an attitude error is ignored since it has been corrected by the

GNSS/SINS integrated system in advance. Thus, the direction cosine matrix C_b^n is only contaminated by the small IMU misalignment error, and it should satisfy

$$\hat{C}_b^n = C_m^n \hat{C}_b^m \approx C_m^n C_b^m (I_3 + [\delta\eta \times]) \quad (5)$$

where I_3 is identity matrix, $[\alpha \times]$ denotes the skew-symmetric matrix obtained by the element of vector α .

Combining (4) and (5), the velocity expressed in n -frame with errors of odometer scale factor and IMU misalignment is achieved as

$$\hat{V}_O^n = \hat{C}_b^n \hat{V}_O^b \approx C_m^n C_b^m ((1 + \delta\bar{k}_O) I_3 + [\delta\eta \times]) V_O^b \quad (6)$$

where the second order items are omitted. Then, subtracting (2) from (6) leads to

$$\delta V_O^n = \hat{V}_O^n - V_O^n \approx -C_b^n [V_O^b \times] \delta\eta + \delta\bar{k}_O C_b^n V_O^b \quad (7)$$

where δV_O^n denotes the velocity error calculated by an odometer and expressed in n -frame.

Same as the SINS position errors dynamic [27], the position error propagation equation of the odometer is obtained as

$$\begin{aligned} \delta \dot{P}_O^n &= -[\omega_{enO}^n \times] \delta P_O^n + \delta V_O^n \\ &\approx -[\omega_{enO}^n \times] \delta P_O^n - C_b^n [V_O^b \times] \delta\eta + \delta\bar{k}_O C_b^n V_O^b \end{aligned} \quad (8)$$

where δP_O^n is the position error calculated by an odometer and expressed in n -frame, $\delta \dot{P}_O^n$ is the derivative of δP_O^n , and ω_{enO}^n is the angular rate of n -frame with respect to e -frame expressed in n -frame. The expansion of term $[V_O^b \times] \delta\eta$ in (8) is obtained as

$$[V_O^b \times] \delta\eta = \begin{bmatrix} 0 & 0 & 0 \\ 0 & 0 & -V_O \\ 0 & V_O & 0 \end{bmatrix} \begin{bmatrix} \delta\eta_x \\ \delta\eta_y \\ \delta\eta_z \end{bmatrix} = V_O \begin{bmatrix} 0 \\ -\delta\eta_y \\ \delta\eta_z \end{bmatrix} \quad (9)$$

where the misalignment error component $\delta\eta_x$ is omitted. Thus, $\delta\eta_x$ is unobservable and can be removed from (8) to simply the equation.

2.3. State and observation equation

The calibration of the odometer scale factor and IMU misalignment is processed by a Kalman filter. The error state vector X_O is comprised of δP_O^n , $\delta \bar{\eta} = [\delta\eta_y \quad \delta\eta_z]^T$, and $\delta\bar{k}_O$, where $\delta \bar{\eta}$ and $\delta\bar{k}_O$ are modeled as a constant and a random walk process, respectively. The state equation is given by

$$\begin{aligned} \dot{X}_O(t) &= \begin{bmatrix} -[\omega_{enO}^n \times] & -C_b^n M & C_b^n V_O^b \\ \mathbf{0}_{2 \times 3} & \mathbf{0}_{2 \times 3} & \mathbf{0}_{2 \times 1} \\ \mathbf{0}_{1 \times 3} & \mathbf{0}_{1 \times 3} & 0 \end{bmatrix} \begin{bmatrix} \delta P_O^n \\ \delta \bar{\eta} \\ \delta\bar{k}_O \end{bmatrix} \\ &+ \begin{bmatrix} \mathbf{0}_{3 \times 1} \\ \mathbf{0}_{2 \times 1} \\ w_{\bar{k}_O} \end{bmatrix} \end{aligned} \quad (10)$$

where $M = \begin{bmatrix} 0 & 0 \\ 0 & -V_O \\ V_O & 0 \end{bmatrix}$, and $w_{\bar{k}_O}$ is a white Gaussian noise.

The first kind of observation used here is the position error, which is given by

$$Z_{OG,k} = P_{O,k}^n - P_{GS,k}^n = H_{OG,k} X_{O,k} + v_{OG,k} \quad (11)$$

where P_{GS}^n is the position expressed in n -frame with the subscript means it is calculated by the GNSS/SINS integrated system, $H_{OG,k} = [I_3 \quad \mathbf{0}_{3 \times 3}]$ is the observation matrix, and $v_{OG} \sim N(\mathbf{0}_{3 \times 1}, R_{OG})$ is the observation noise. To achieve good performance, this observation can be applied when GNSS signals are available with high quality.

The second kind of observation is the velocity error derived from the velocity assumption of NHC. Let \hat{V}^b denote the calculated vehicle velocity expressed in b -frame, and thus the velocity error is given by

$$\delta V^b = \hat{V}^b - V^b = \hat{C}_n^b V^n - V^b = [V^b \times] \delta\eta \quad (12)$$

where $\hat{C}_n^b = (I_3 - [\delta\eta \times]) C_m^n C_n^m$ denotes the transpose of \hat{C}_b^n in (5). Accordingly, the observation equation is obtained as

$$Z_{ON,k} = \begin{bmatrix} \hat{V}_{GSy,k}^b - V_{NHCy,k}^b \\ \hat{V}_{GSz,k}^b - V_{NHCz,k}^b \end{bmatrix} = H_{ON,k} X_{O,k} + v_{ON,k} \quad (13)$$

where \hat{V}_{GSy}^b and \hat{V}_{GSz}^b are the velocity components of $\hat{V}_{GS}^b = \hat{C}_b^n V_{GS}^n$ with V_{GS}^n denotes the GNSS/SINS integrated vehicle velocity, $\begin{bmatrix} V_{NHCy}^b \\ V_{NHCz}^b \end{bmatrix} = \mathbf{0}_{2 \times 1}$ denotes the velocity constraint

obtained by NHC, $H_{ON} = \begin{bmatrix} \mathbf{0}_{1 \times 3} & 0 & -\hat{V}_{GSx}^b & 0 \\ \mathbf{0}_{1 \times 3} & \hat{V}_{GSx}^b & 0 & 0 \end{bmatrix}$ is the observation matrix, and $v_{ON} \sim N(\mathbf{0}_{2 \times 1}, R_{ON})$ is the observation noise. This observation can be applied when the vehicle conforms to NHC strictly. Moreover, it can be readily found that only IMU misalignment is observable in (13), thus observation in (11) is essential to calibrate the scale factor.

It should be noted that the redundant observations shown above are utilized selectively. The first kind of observation is utilized when high-quality GNSS signals are received. Whereas, the second kind of observation is utilized when a rectilinear motion is detected. If two observations are both available, sequential Kalman filter is applied to fuse these observations.

3. Velocity compensation

In the classical calibration algorithm, the lever arm error is also included in the state error vector and estimated by a Kalman filter using a centralized system structure [23]. The observation equation of the centralized system is given by [23]

$$\begin{aligned} Z_{OV,k} &\approx C_n^b \delta V^n - C_n^b [V^n \times] \delta\varphi \\ &+ [V^b \times] \delta\eta - \delta\bar{k}_O V^b - C_m^b [\omega_{em}^m \times] l^m \end{aligned} \quad (14)$$

where l^m denotes the lever arm, and ω_{em}^m denotes the angular velocity of the IMU relative to the earth. It can be readily found

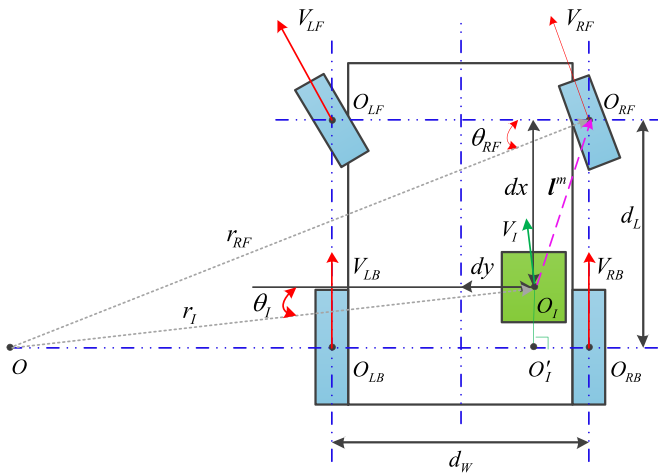


Figure 2. The relative position and measured velocities of the IMU and four odometers when the vehicle turns left according to the Ackermann steering geometry.

that ω_{em}^m may be close to zero and remain constant when the land vehicle conforms to NHC and makes no turning manoeuvres. To achieve the estimation of lever arm error, a high-precision gyroscope and some angular motions which violate NHC are unavoidable. Therefore, for a low-cost MEMS-based IMU, the velocity error caused by the lever arm is best compensated by a tape measure and a compensation model.

Figure 2 illustrates the relative positions and measured velocities of the IMU and four odometers when the vehicle turns left according to the Ackermann steering geometry. The rotation center O is on the extension cord of the rear axle. O_{LF} , O_{LF} , O_{LB} , and O_{RB} are the mounting centers of the four odometers, respectively. V_{LF} , V_{RF} , V_{LB} , and V_{RB} are the corresponding measured velocities, respectively. O_I and V_I are the mounting center and turning velocity of the IMU, respectively. l^m denotes the lever arm between the IMU and the odometer mounted on the right front wheel, which can be represented by the X -axis offset dx and Y -axis offset dy of the IMU. It shows that the velocity measured at the center of each wheel is different from the velocity measured at the center of the IMU. Furthermore, the velocity of the steered wheel does not point forward when the vehicle makes a turn, which violates the assumption of the odometer measurement model in (1). Therefore, the original velocity measured by the odometer should be compensated to improve the fusion performance.

3.1. Lever arm compensation for the odometer measurement

The odometer mounted on the center of the right front wheel is taken as an example. When the vehicle turns left, the measured velocity V_{RF} is perpendicular to the turning radius r_{RF} . From figure 2, the forward velocity component at the center of the right front wheel is obtained as

$$V_{RFx} = V_{RF} \cos \theta_{RF} = \sqrt{V_{RF}^2 - \omega^2 d_L^2} \quad (15)$$

where d_L represents the wheel base, ω denotes the turning angular rate, and θ_{RF} is the steering angle that satisfies

$$\sin \theta_{RF} = \frac{d_L}{r_{RF}} = \frac{d_L \omega}{V_{RF}}. \quad (16)$$

Let ω^m denote the angular velocity measured by the IMU, and thus ω can be obtained by taking the absolute value of the third element of $C_m^b \omega^m$. Due to the existence of the lever arm, the forward velocity component V_{RFx} does not coincide with the forward velocity component at the center of the IMU. From figure 2, the forward velocity component at the IMU center obtained by the odometer mounted on the right front wheel is calculated as

$$V_{Ix_RF} = V_I \cos \theta_I = V_{RFx} - \omega \left(\frac{d_w}{2} - dy \right) \quad (17)$$

where d_w denotes the wheel track, and θ_I is the steering angle that satisfies

$$\cos \theta_I = \frac{\sqrt{\left(\frac{V_{RF}}{\omega} \right)^2 - d_L^2} - \left(\frac{d_w}{2} - dy \right)}{r_I}. \quad (18)$$

Equation (17) is the velocity compensation model for the odometer mounted on the right front wheel, and the compensation model for the odometer mounted on the left front wheel can be obtained similarly. Whereas, for the odometer mounted on the non-steered wheel, only the second compensation step is required since it has measured the forward velocity. Moreover, when the vehicle turns right, the same result can be obtained.

3.2. Lateral velocity compensation

As shown in figure 2, the lateral velocity component at the center of the IMU is not zero when the vehicle is turning, which violates the assumption of NHC adopted in the velocity measurement model in (1). To apply the NHC accurately, the lateral velocity component at the center of the IMU should be removed from the converted velocity.

According to the geometric relationship in figure 2, the absolute value of the lateral velocity component at the center of the IMU can be calculated as follows

$$|V_{Iy}| = V_I \sin \theta_I = V_I \frac{d_L - dx}{r_I} = \omega (d_L - dx) \quad (19)$$

where the sign of V_{Iy} is decided according to the turning direction and the definition of VBF. By removing the lateral velocity component from the converted velocity, the application of NHC can be extended. Notable, to achieve accurate compensation by (17) and (19), the drifts of the gyroscope should be well processed. For example, heuristic drift reduction can be applied to reduce the drift of gyro [22].

where $\hat{\mathbf{C}}_n^b = \mathbf{C}_m^b \hat{\mathbf{C}}_n^m = \mathbf{C}_m^b \mathbf{C}_n^m (\mathbf{I}_3 + [\delta\varphi \times])$ denotes the direction cosine matrix contaminated by the attitude error. Let $\hat{\mathbf{V}}_S^b = \hat{\mathbf{C}}_n^b \mathbf{V}_S^n = \begin{bmatrix} \hat{V}_{Sx}^b & \hat{V}_{Sy}^b & \hat{V}_{Sz}^b \end{bmatrix}^T$ denote the SINS velocity expressed in b -frame and it is contaminated by the attitude error. According to (26), the observation equation is written as

$$\mathbf{Z}_{OV,k} = \hat{V}_{Sx,k}^b - V_{O,k}(k) = \mathbf{H}_{OV,k} \mathbf{X}_k + \mathbf{v}_{OV,k} \quad (27)$$

where V_O denotes the forward velocity provided by the odometer, $\mathbf{H}_{OV} = \begin{bmatrix} \mathbf{0}_{1 \times 3} & \mathbf{A} & \mathbf{B} & \mathbf{0}_{1 \times 6} \end{bmatrix}$ represents the observation matrix with $\mathbf{A} = \begin{bmatrix} \hat{\mathbf{C}}_{11} & \hat{\mathbf{C}}_{12} & \hat{\mathbf{C}}_{13} \end{bmatrix}$ and $\mathbf{B} = \begin{bmatrix} \hat{V}_{Sx}^n \hat{\mathbf{C}}_{12} - \hat{V}_{Sy}^n \hat{\mathbf{C}}_{13} & \hat{V}_{Sx}^n \hat{\mathbf{C}}_{13} - \hat{V}_{Sz}^n \hat{\mathbf{C}}_{11} & \hat{V}_{Sy}^n \hat{\mathbf{C}}_{11} - \hat{V}_{Sx}^n \hat{\mathbf{C}}_{12} \end{bmatrix}$, $\hat{\mathbf{C}}_{ij}$ is the $[i,j]$ element of $\hat{\mathbf{C}}_n^b$, and $\mathbf{v}_{OV} \sim \mathcal{N}(0, \mathbf{R}_{OV})$ denotes the observation noise.

4.3. Motion aided constraints

MACs can provide virtual velocity observation according to the motion and driving information of the vehicle to mitigate SINS errors. Two general MACs, namely zero velocity update (ZUPT) and NHC, are applied in this system. The state equation is the same as the one used in the GNSS/SINS LC integrated system.

ZUPT assumes that the velocity of the vehicle should be zero when the vehicle is stationary. Thus, the observation equation of ZUPT can be written as

$$\mathbf{Z}_{Z,k} = \mathbf{V}_{S,k}^n - \mathbf{0}_{3 \times 1} = \mathbf{H}_{Z,k} \mathbf{X}_k + \mathbf{v}_{Z,k} \quad (28)$$

where $\mathbf{H}_Z = \begin{bmatrix} \mathbf{0}_{3 \times 3} & \mathbf{I}_3 & \mathbf{0}_{3 \times 9} \end{bmatrix}$ represents the observation matrix, and $\mathbf{v}_Z \sim \mathcal{N}(\mathbf{0}_{3 \times 1}, \mathbf{R}_Z)$ denotes the observation noise.

The velocity assumption of NHC has been discussed in the calibration procedure. The observation equation of NHC is also obtained from the velocity error in (26), and it is given by

$$\mathbf{Z}_{N,k} = \begin{bmatrix} \hat{V}_{Sy,k}^b - V_{NHCy,k}^b \\ \hat{V}_{Sz,k}^b - V_{NHCz,k}^b \end{bmatrix} = \mathbf{H}_{N,k} \mathbf{X}_k + \mathbf{v}_{N,k} \quad (29)$$

where $\mathbf{H}_N = \begin{bmatrix} \mathbf{0}_{2 \times 3} & \mathbf{A} & \mathbf{B} & \mathbf{0}_{2 \times 6} \end{bmatrix}$ denotes the observation matrix with $\mathbf{A} = \begin{bmatrix} \hat{\mathbf{C}}_{21} & \hat{\mathbf{C}}_{22} & \hat{\mathbf{C}}_{23} \\ \hat{\mathbf{C}}_{31} & \hat{\mathbf{C}}_{32} & \hat{\mathbf{C}}_{33} \end{bmatrix}$ and $\mathbf{B} = \begin{bmatrix} \hat{V}_{Sx}^n \hat{\mathbf{C}}_{22} - \hat{V}_{Sy}^n \hat{\mathbf{C}}_{23} & \hat{V}_{Sx}^n \hat{\mathbf{C}}_{23} - \hat{V}_{Sz}^n \hat{\mathbf{C}}_{21} & \hat{V}_{Sy}^n \hat{\mathbf{C}}_{21} - \hat{V}_{Sx}^n \hat{\mathbf{C}}_{22} \\ \hat{V}_{Sx}^n \hat{\mathbf{C}}_{32} - \hat{V}_{Sy}^n \hat{\mathbf{C}}_{33} & \hat{V}_{Sx}^n \hat{\mathbf{C}}_{33} - \hat{V}_{Sz}^n \hat{\mathbf{C}}_{31} & \hat{V}_{Sy}^n \hat{\mathbf{C}}_{31} - \hat{V}_{Sx}^n \hat{\mathbf{C}}_{32} \end{bmatrix}$, $\hat{\mathbf{C}}_{ij}$ is the $[i,j]$ element of $\hat{\mathbf{C}}_n^b$, and $\mathbf{v}_N \sim \mathcal{N}(\mathbf{0}_{2 \times 1}, \mathbf{R}_N)$ denotes the observation noise. Observation equations in (27) and (29) can be combined when the land vehicle conforms to NHC and an odometer is utilized.

4.4. Sequential Kalman filter

All multi-observations are processed by a sequential Kalman filter, which can avoid the computation of high-dimensional inverse matrices and facilitate the resilient fusion system. It

can be proved that the sequential processing is functionally equivalent to the batch processing in the case of uncorrelated observation noises, and it can save over 30% computation compared to the batch processing.

Generally, the sequential Kalman filter can be applied to the multi-information system which shares the same state equation and uncorrelated observation noises. If there are M sensors in the system, the system model of the multi-information fusion system is written as

$$\begin{cases} \mathbf{X}_k = \Phi_{k/k-1} \mathbf{X}_{k-1} + \Gamma_{k/k-1} \mathbf{w}_{k-1} \\ \mathbf{Z}_{i,k} = \mathbf{H}_{i,k} \mathbf{X}_k + \mathbf{v}_{i,k} \end{cases} \quad (30)$$

where $i = 1, \dots, M$, $\mathbf{X}_k \in \mathcal{R}^n$ denotes the state vector at epoch k , $\Phi_{k/k-1} \in \mathcal{R}^{n \times n}$ represents the state transition matrix, $\Gamma_{k/k-1} \in \mathcal{R}^{n \times p}$ denotes the system noise distribution matrix, $\mathbf{w}_{k-1} \in \mathcal{R}^p$ is the system noise, $\mathbf{Z}_{i,k} \in \mathcal{R}^{m_i}$, $\mathbf{H}_{i,k} \in \mathcal{R}^{m_i \times n}$ and $\mathbf{v}_{i,k} \in \mathcal{R}^{m_i}$ represent the observation, observation matrix and observation noise of the i -th sensor, respectively.

The sequential processing at each epoch is implemented with the following steps.

Step 1: Time update

$$\begin{cases} \hat{\mathbf{X}}_{k/k-1} = \Phi_{k/k-1} \hat{\mathbf{X}}_{k-1} \\ \mathbf{P}_{k/k-1} = \Phi_{k/k-1} \mathbf{P}_{k-1} \Phi_{k/k-1}^T + \Gamma_{k/k-1} \mathbf{Q}_{k-1} \Gamma_{k/k-1}^T \end{cases} \quad (31)$$

where $\hat{\mathbf{X}}_{k/k-1}$ denotes the one-stage predicted state vector, $\hat{\mathbf{X}}_{k-1}$ denotes the estimated state vector in the previous epoch, $\mathbf{P}_{k/k-1}$ represents the predicted state error covariance matrix, \mathbf{P}_{k-1} is the state error covariance matrix in the previous epoch, and $\mathbf{Q}_{k-1} \in \mathcal{R}^{p \times p}$ denotes the system noise covariance.

Step 2: Initialization of the observation update loop

$$\begin{cases} \hat{\mathbf{X}}_{0,k} = \hat{\mathbf{X}}_{k/k-1} \\ \mathbf{P}_{0,k} = \mathbf{P}_{k/k-1} \end{cases} \quad (32)$$

where $\hat{\mathbf{X}}_{0,k}$ and $\mathbf{P}_{0,k}$ are the initial state vector and initial state error covariance matrix of the observation update loop, respectively.

Step 3: Observation update loop for each observation

$$\begin{cases} \mathbf{K}_{i,k} = \mathbf{P}_{i-1,k} \mathbf{H}_{i,k}^T (\mathbf{H}_{i,k} \mathbf{P}_{i-1,k} \mathbf{H}_{i,k}^T + \mathbf{R}_{i,k})^{-1} \\ \hat{\mathbf{X}}_{i,k} = \hat{\mathbf{X}}_{i-1,k} + \mathbf{K}_{i,k} (\mathbf{Z}_{i,k} - \mathbf{H}_{i,k} \hat{\mathbf{X}}_{i-1,k}) \\ \mathbf{P}_{i,k} = (\mathbf{I} - \mathbf{K}_{i,k} \mathbf{H}_{i,k}) \mathbf{P}_{i-1,k} \end{cases} \quad (33)$$

where i denotes the index increased from 1 to M , $\mathbf{K}_{i,k}$ represents the Kalman gain matrix of the i -th observation, and $\mathbf{R}_{i,k} \in \mathcal{R}^{m_i \times m_i}$ is the noise covariance of the i -th observation.

Step 4: Acquisition of the observation update result

$$\begin{cases} \hat{\mathbf{X}}_k = \hat{\mathbf{X}}_{M,k} \\ \mathbf{P}_k = \mathbf{P}_{M,k} \end{cases} \quad (34)$$

where $\hat{\mathbf{X}}_k$ and \mathbf{P}_k are the estimated state vector and state error covariance matrix in this epoch, respectively.

Benefit from the decentralized system architecture and sequential Kalman filter, the multi-source information fusion

system can conveniently process different observations in different driving environments.

5. Experimental validation and analysis

A real road test was carried out in Guangzhou to verify the effectiveness of the proposed system. As is shown in figure 4, there are lots of highway overpasses, elevated walkways, dense trees and tunnels on the route, which helps to construct the required experimental scenario including GNSS open areas and GNSS signals blocked areas. The whole experiment takes 1460 s, and there is a stationary state of 380 s at the beginning. The two tunnels on the route are about 1.6 km long (the Clifford Tunnel) and 1.2 km long (the Zhongcun Tunnel), respectively.

The reference system comprises a fiber optic gyro IMU (KVH1750, 200 Hz) and a GNSS receiver (Trimble BD990, 1 Hz). The reference solution is generated in differential mode by the commercial software (Inertial Explorer) at the rate of 1 Hz, and its positioning and attitude measurement accuracies are claimed to be at the centimeter-level and 0.015° , respectively.

The evaluated system uses a MEMS-based IMU (ADIS 16 505, 100 Hz), a GNSS receiver (UBLOX-F9P, 1 Hz) and a wheel encoder (20 Hz). The main physical characteristics of the ADIS 16 505 IMU are summarized in table 1. The wheel encoder is installed on the center of the right front wheel, which can maintain a velocity measurement accuracy better than 0.2 m s^{-1} . The number of satellites observed by the evaluated system is presented in figure 5. As is shown in figure 5, the GNSS signals are relatively poor at the first 100 s after the car starts to move. Besides, the GNSS signals are totally cut off for 88 s (885 s-972 s) and 68 s (1019 s-1086 s) when the vehicle goes through two tunnels, respectively.

5.1. Real time calibration and compensation

The calibration and compensation results are presented in this section. To elaborate the effectiveness of the proposed method, the estimation results are compared with the results obtained by the centralized method using velocity-level observation in [23]. In the centralized structure, the state vector consists of 15-dimensional SINS error state and 6-dimensional odometer error state. The observation is made up of the velocity error calculated by the SINS and odometer in the b -frame in (14), as well as the position and velocity error calculated by the SINS and GNSS in the n -frame.

The initial scale factor is set as 1 and the calibration begins at 391 s. Figure 6 shows the odometer scale factor estimated by the centralized and decentralized method, respectively. As plotted by red lines in figure 6, the odometer scale factor estimated by the decentralized structure using the position-level observation converges rapidly and steadily. Although the centralized structure can estimate the scale factor through the velocity-level observation no matter GNSS signals are available or not, the velocity provided by the low-cost SINS is not accurate enough to calibrate the odometer scale factor

precisely. Especially, when GNSS signals are cut off, the velocity information provided by the stand-alone SINS may result in incorrect estimation of the odometer scale factor, which is shown in the grey block. Thus, to achieve accurate estimation of the scale factor for the application of low-cost GNSS/SINS/odometer fusion system, the decentralized structure using position-level observation is more suitable.

The IMU misalignment estimations are shown in figure 7. Compared with the centralized structure, the decentralized system can estimate the IMU misalignment more rapidly by using the GNSS/SINS integrated position information as the observation. It shows that the Y -axis misalignment and Z -axis misalignment converge at about 2.25° and 0.5° , respectively, which demonstrates that the IMU is not perfectly mounted. Directly converting the velocity provided by an odometer or NHC using the direction cosine matrix may result in significant vertical and horizontal velocity errors. The Z -axis misalignment estimation accuracy of the decentralized system may be slightly worse since the calibration may be suspended during several turning sections where GNSS signals are unavailable. Therefore, to estimate Z -axis misalignment more accurately, enough turning maneuvers in GNSS open areas are required.

Figure 8 presents the curve of estimated lever arm obtained by the traditional centralized method. The measured lever arm is [3.196, 0.964, 0.82] m. However, the estimated result is around zero, which indicates that the small coefficient of the lever arm error state in the centralized structure makes it difficult to estimate the real value. Moreover, the unobservable error state may influence the convergence process when GNSS signals are poor. In other words, the velocity error caused by the lever arm should be compensated by a velocity model instead of a real-time estimation when using a low-cost SINS. To verify this claim, the forward velocity errors obtained respectively by calibrating the odometer scale factor and compensating the lever arm, are compared in figure 9. It shows that by compensating the lever arm, the forward velocity error is mitigated when the vehicle turns. Moreover, from the raw forward velocity error plotted by the black line, it can be concluded that the odometer scale factor error has a greater impact on the velocity estimation accuracy since it brings mean velocity error of about 0.2 m s^{-1} . Statistical results of the forward velocity errors are presented in table 2. The root-mean-square error (RMSE) is improved by 56.3% after the calibration of odometer scale factor and finally improved by 62.5% after both the calibration of odometer scale factor and the compensation of lever arm.

5.2. Performance of the GNSS/SINS/odometer fusion system

Positioning result and discussions of the proposed GNSS/SINS/odometer resilient fusion system are presented in this section.

Figure 10 presents the positioning result of the centralized system and that of the decentralized fusion system at two tunnels, where GNSS signals are totally unavailable. It shows that benefiting from the decentralized structure, the calculated trajectory can track the referenced trajectory more



Figure 4. Car test route, road environments, and number of satellites received by the reference system.

Table 1. Main physical characteristics of the ADIS 16 505 IMU.

Parameter	Gyroscope	Accelerometer
In-run bias stability (1σ)	$\leq 2.3^\circ \text{ h}^{-1}$	$\leq 4.4 \times 10^{-5} \text{ m s}^{-2}$
Angular random walk (1σ)	$\leq 0.19^\circ \sqrt{\text{hr}^{-1}}$	$0.012 \text{ m s}^{-1} \sqrt{\text{hr}}$

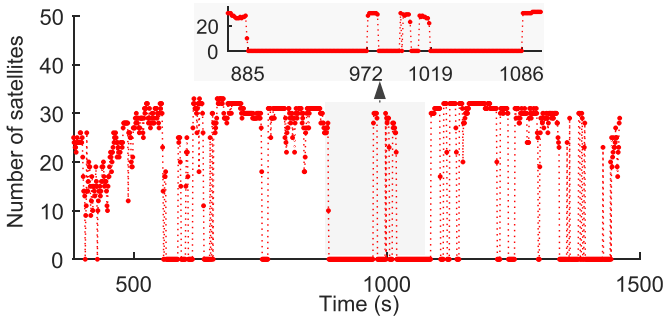


Figure 5. Number of satellites observed by the evaluated system.

exactly at two tunnels. Figure 11 demonstrates the positioning errors of two system structures during the whole trajectory. The blue line indicates that the fusion of GNSS, SINS and odometer information in the centralized structure influences the convergence of the positioning error when GNSS signals are available. Moreover, the calibration of odometer scale factor during GNSS signal outages by the centralized system cannot obtain satisfactory performance on the horizontal direction. However, the proposed decentralized system achieves better performance when GNSS signals are unavailable by directly using the previously estimated parameters. Although the centralized structure can artificially suspend the feedback correction of the parameters during GNSS signals outages, the previously estimated value may be inaccurate due

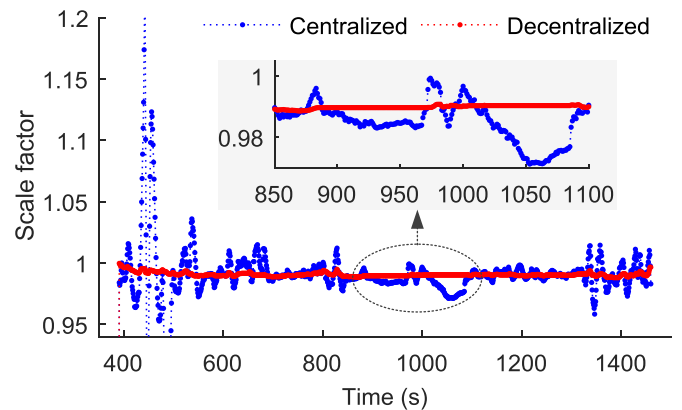


Figure 6. Comparison of the estimation results of the odometer scale factor.

to the velocity-level observation it used, and it may influence the estimation of other error states. The positioning RMSE during the whole trajectory is summarized in table 3. It shows that compared with the centralized structure, the positioning RMSE in the east and north direction are improved by 78.5% and 80.4%, respectively. Table 4 summarizes the average positioning RMSE at two tunnels. It shows that the average horizontal positioning RMSE at two tunnels has been mitigated from 7.46 m to 0.93 m by the decentralized fusion structure, which verifies the effectiveness of the proposed system in short GNSS signal blockage environment.

Figure 12 shows the comparison of velocity errors of two system structure during the whole trajectory. It is demonstrated that the horizontal velocity in the centralized system has a relatively larger error in GNSS-denied environment, which is caused by the misestimated odometer scale factor obtained by the inaccurate velocity-level observation.

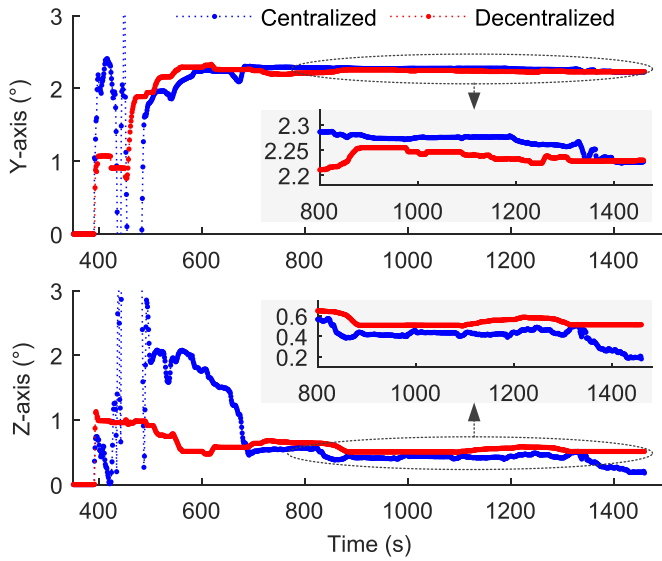


Figure 7. Estimation result of the IMU misalignment.

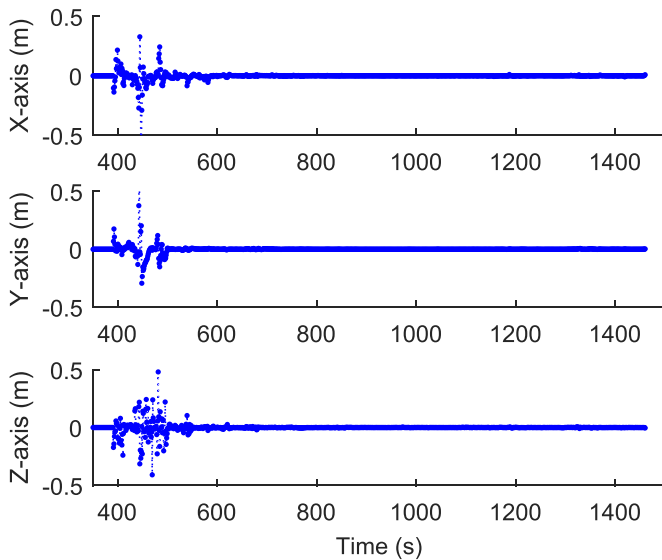


Figure 8. Estimation result of the lever arm obtained by the centralized method.

Furthermore, the velocity error converges slower than that in the decentralized system. However, a relatively small horizontal velocity error is achieved by the decentralized system when GNSS signals are unavailable by utilizing the previously estimated odometer scale factor. Statistical results in table 5 show that the velocity RMSE in the north and east direction have been reduced from 0.25 m s^{-1} and 0.28 m s^{-1} to 0.06 m s^{-1} and 0.06 m s^{-1} by the decentralized system, respectively.

Figure 13 illustrates the comparison of attitude errors of two system structure during the whole trajectory. It indicates that the proposed decentralized system structure has a relative better performance on the estimation of pitch and roll angles. Whereas, the centralized structure has a better performance

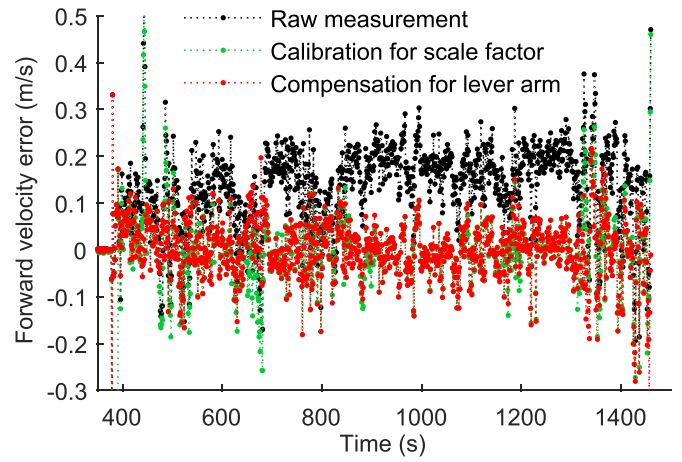


Figure 9. Comparison of the forward velocity errors.

Table 2. Estimation errors of the forward velocity.

Errors (m s^{-1})	RMSE	Improve
Raw	0.16	—
Scale factor	0.07	56.3%
Scale factor and lever arm	0.06	62.5%

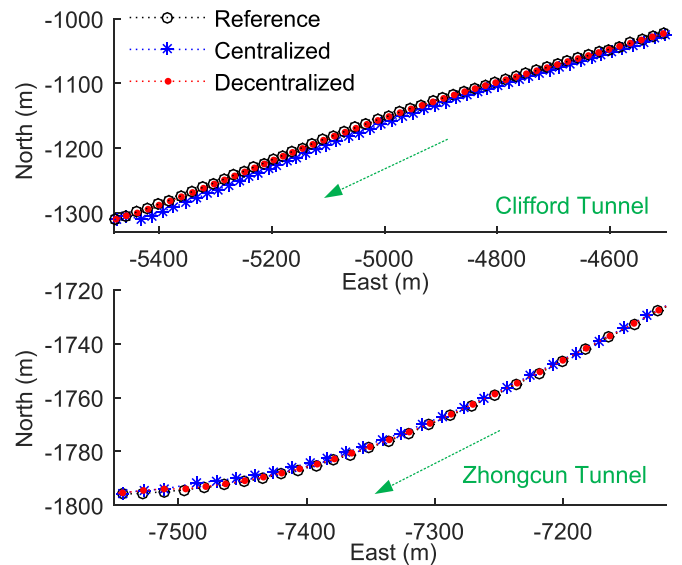


Figure 10. Comparison of the positioning results at two tunnels.

on the estimation of yaw angle at the end of the trajectory. The reason is that the Z-axis IMU misalignment can still be estimated by the centralized structure when turning maneuvers occur during GNSS signal outages. It should be pointed that the decentralized system can also obtain a good estimation of yaw angle as long as enough turning maneuvers occur when GNSS signals are available. Table 6 shows that the pitch and roll attitude RMSE have been mitigated from 0.65° and 0.48° to 0.28° and 0.26° by the decentralized system, respectively.

To sum up, the centralized structure is not feasible for a low-cost GNSS/SINS/odometer integration system since it

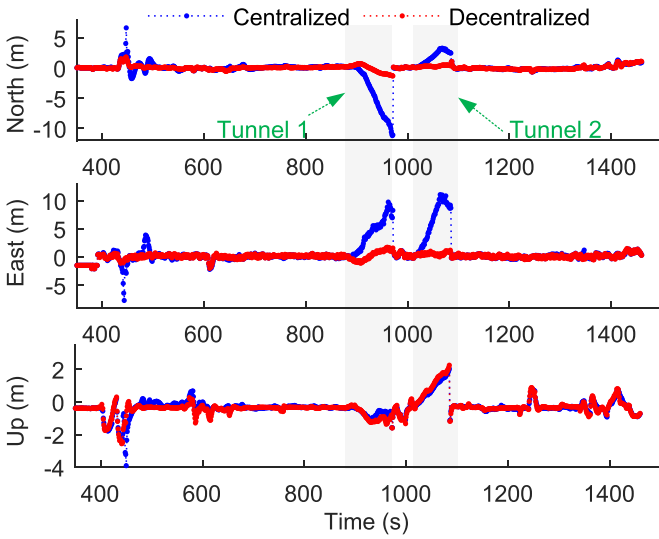


Figure 11. Comparison of the positioning errors in the north, east and up direction during the whole trajectory.

Table 3. Comparison of the position RMSE during the whole trajectory.

RMSE (m)	Centralized	Decentralized	Improve
North	1.72	0.37	78.5%
East	2.40	0.47	80.4%
Horizontal	2.95	0.59	80.0%

Table 4. Comparison of the average positioning RMSE at two tunnels.

RMSE (m)	Centralized	Decentralized	Improve
North	3.78	0.51	86.5%
East	6.11	0.77	87.4%
Horizontal	7.46	0.93	87.5%

not only influences the convergence of the error state but also cannot provide enough accurate velocity-level observation to calibrate the odometer scale factor even when GNSS signals are available. The decentralized structure can achieve a better performance on the estimation of position and velocity no matter the GNSS signals are available or not. It calibrates the parameters through accurate GNSS/SINS integrated position information when GNSS signals are available and applies these parameters in SINS/odometer system during GNSS signals outages. Notably, to obtain better Z-axis misalignment and yaw estimation, enough turning maneuvers are required for the decentralized system when GNSS signals are available.

To illustrate the necessity of the lateral velocity compensation when applying NHC, comparison of the velocity errors at the Clifford tunnel are presented in figures 14 and 15, respectively. It can be seen from figure 4 that there is an east-west curve at the entrance of the Clifford tunnel, hence the lateral velocity component of the vehicle

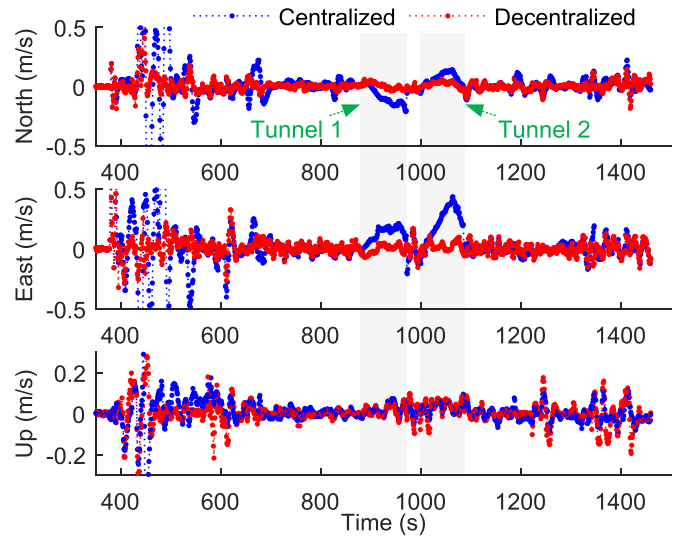


Figure 12. Comparison of the velocity errors in the north, east and up direction during the whole trajectory.

Table 5. Comparison of the velocity RMSE during the whole trajectory.

RMSE (m s ⁻¹)	Centralized	Decentralized	Improve
North	0.25	0.06	76.0%
East	0.28	0.06	78.6%
Up	0.07	0.06	14.3%

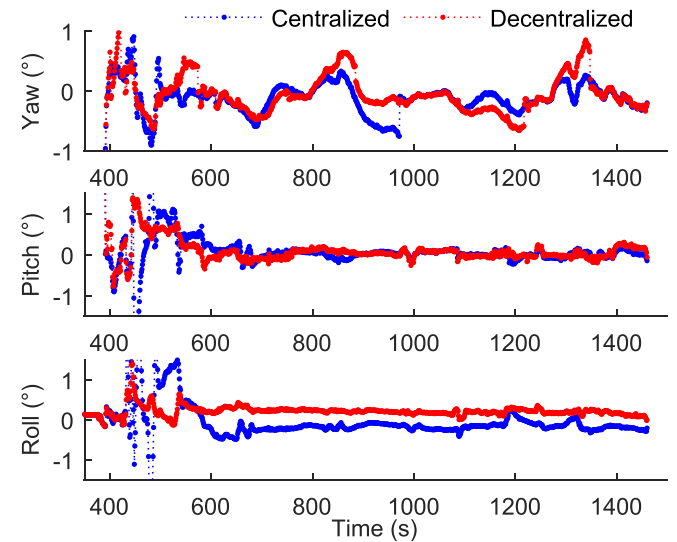


Figure 13. Comparison of the attitude errors during the whole trajectory.

should not be zero. As is shown in figures 14 and 15, the velocity error and position error in the north direction have been significantly mitigated with the compensation of lateral velocity component. Tables 7 and 8 present the velocity and position RMSE, respectively. It shows that with the compensation of lateral velocity component when applying NHC, the velocity and position accuracy in the north direction have been improved by 44.9% and 66.5%, respectively. Therefore, the

Table 6. Comparison of the attitude RMSE during the whole trajectory.

RMSE (°)	Centralized	Decentralized	Improve
Yaw	0.28	0.35	/
Pitch	0.65	0.28	56.9%
Roll	0.48	0.26	45.8%

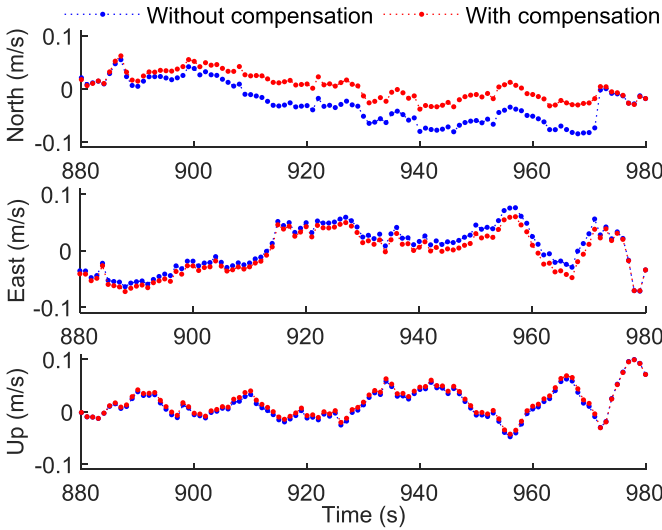


Figure 14. Comparison of the velocity errors with and without lateral velocity compensation at the Clifford tunnel.

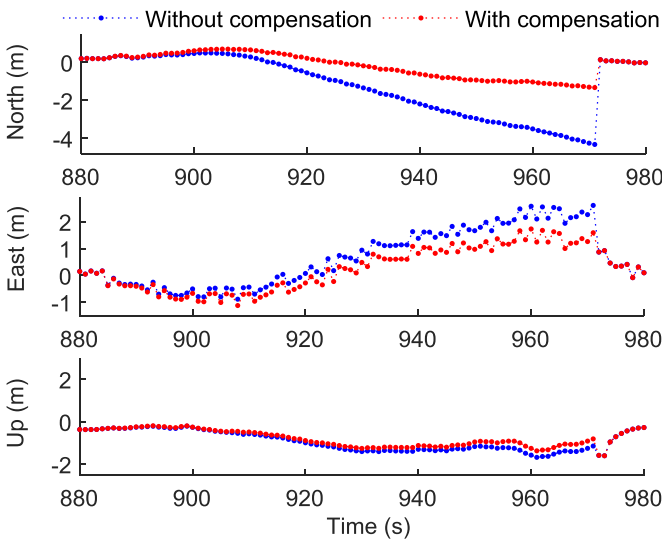


Figure 15. Comparison of the positioning errors with and without lateral velocity compensation at the Clifford tunnel.

lateral velocity compensation model can significantly mitigate the velocity and position errors when NHC is combined with an odometer to provide 3D velocity constraint during turning manoeuvres.

Table 7. Comparison of the velocity RMSE with and without lateral velocity compensation at the Clifford tunnel.

RMSE (m s ⁻¹)	Without compensation	With compensation	Improve
North	0.049	0.027	44.9%
East	0.038	0.036	5.3%

Table 8. Comparison of the position RMSE with and without lateral velocity compensation at the Clifford tunnel.

RMSE (m)	Without compensation	With compensation	Improve
North	2.12	0.71	66.5%
East	1.33	0.90	32.3%
Horizontal	2.51	1.14	54.6%

6. Conclusions

In this paper, we attempt to improve the performance of the low-cost GNSS/SINS integrated land vehicle navigation system in a GNSS-denied environment by selectively combining the measurements from the odometer and motion aided constraints. To achieve high precision, a real-time calibration algorithm based on the odometer position error propagation equation is proposed, which can estimate both the odometer scale factor and IMU misalignment when high-quality GNSS signals are available. Meanwhile, a velocity compensation model is established to compensate the velocity measurement errors generated by the lever arm and turning motions. To facilitate the selective fusion of multi-source information, a decentralized system architecture is designed and a sequential Kalman filter is adopted. The real car experiment verifies the effectiveness of the proposed calibration and compensation strategy. It shows that the average horizontal positioning RMSE is 0.93 m when GNSS signals are cut off for 88 s and 68 s at two tunnels, which proves that the designed GNSS/SINS/odometer fusion system can maintain a 2D positioning RMSE of one-meter level in short GNSS-denied environments. Compared with the traditional centralized structure, the designed decentralized system has better performance no matter GNSS signals are available or unavailable. This study is meaningful for the application of low-cost land vehicle navigation systems in complex urban environments. To further improve the horizontal positioning performance, we will study the fusion system implemented by multi-odometers in future work.

Data availability statement

The data generated and/or analysed during the current study are not publicly available for legal/ethical reasons but are available from the corresponding author on reasonable request.

Acknowledgments

The project is supported by the National Science Foundation of China (Grant Nos. 42274037 and 41874034), the National key research and development program of China (Grant No. 2020YFB0505804), and the Beijing Natural Science Foundation (Grant No. 4202041). In addition, the authors would like to thank Beijing Hi-Star Navigation Technology Co. Ltd, for sharing the car test data.

ORCID iD

Long Zhao  <https://orcid.org/0000-0001-5761-3498>

References

- [1] Skog I and Händel P 2009 In-car positioning and navigation technologies—a survey *IEEE Trans. Intell. Transp. Syst.* **10** 4–21
- [2] Georgy J, Noureldin A and Goodall C 2012 Vehicle navigator using a mixture particle filter for inertial sensors/odometer/map data/GPS integration *IEEE Trans. Consum. Electron.* **58** 544–52
- [3] Chen W, Li X, Song X, Li B, Song X and Xu Q 2015 A novel fusion methodology to bridge outages for land vehicle positioning *Meas. Sci. Technol.* **26** 075001
- [4] Chen C and Chang G 2020 Low-cost GNSS/INS integration for enhanced land vehicle performance *Meas. Sci. Technol.* **31** 035009
- [5] Li X and Xu Q 2017 A reliable fusion positioning strategy for land vehicles in GPS-denied environments based on low-cost sensors *IEEE Trans. Ind. Electron.* **64** 3205–15
- [6] Li X and Zhang W 2010 An adaptive fault-tolerant multisensor navigation strategy for automated vehicles *IEEE Trans. Veh. Technol.* **59** 2815–29
- [7] Georgy J, Karamat T, Iqbal U and Noureldin A 2011 Enhanced MEMS-IMU/odometer/GPS integration using mixture particle filter *GPS Solut.* **15** 239–52
- [8] Chiang K W, Chang H W, Li Y H, Tsai G J, Tseng C L, Tien Y C and Hsu P C 2020 Assessment for INS/GNSS/odometer/barometer integration in loosely-coupled and tightly-coupled scheme in a GNSS-degraded environment *IEEE Sens. J.* **20** 3057–69
- [9] Zhu J, Tang Y, Shao X and Xie Y 2021 Multisensor fusion using fuzzy inference system for a visual-IMU-wheel odometry *IEEE Trans. Instrum. Meas.* **70** 2505216
- [10] Li X, Wang X, Liao J, Li X, Li S and Lyu H 2021 Semi-tightly coupled integration of multi-GNSS PPP and S-VINS for precise positioning in GNSS-challenged environments *Satell. Navig.* **2** 1–14
- [11] Yue Z, Lian B, Tang C and Tong K 2020 A novel adaptive federated filter for GNSS/INS/VO integrated navigation system *Meas. Sci. Technol.* **31** 085102
- [12] Dissanayake G, Sukkarieh S, Nebot E and Durrantwhyte H 2001 The aiding of a low-cost strapdown inertial measurement unit using vehicle model constraints for land vehicle applications *IEEE Trans. Robot. Autom.* **17** 731–41
- [13] Liu Z, El-Sheimy N, Yu C and Qin Y 2018 Motion constraints and vanishing point aided land vehicle navigation *Micromachines* **9** 249–73
- [14] Li Z, Wang J, Li B, Gao J and Tan X 2014 GPS/INS/odometer integrated system using fuzzy neural network for land vehicle navigation applications *J. Navig.* **67** 967–83
- [15] Li J, Song N, Yang G, Li M and Cai Q 2017 Improving positioning accuracy of vehicular navigation system during GPS outages utilizing ensemble learning algorithm *Inf. Fusion* **35** 1–10
- [16] Chen Q, Zhang Q and Niu X 2021 Estimate the pitch and heading mounting angles of the IMU for land vehicular GNSS/INS integrated system *IEEE Trans. Intell. Transp. Syst.* **22** 6503–15
- [17] Wei O, Wu Y and Chen H 2021 INS/odometer land navigation by accurate measurement modeling and multiple-model adaptive estimation *IEEE Trans. Aerosp. Electron. Syst.* **57** 245–62
- [18] Li L, Sun H, Yang S, Ding X, Wang J, Jiang J, Pu X, Ren C, Hu N and Guo Y 2018 Online calibration and compensation of total odometer error in an integrated system *Measurement* **123** 69–79
- [19] Fu Q, Liu Y, Liu Z, Li S and Guan B 2018 High-accuracy SINS/LDV integration for long-distance land navigation *IEEE Trans. Mechatron.* **23** 2952–62
- [20] Syed Z F, Aggarwal P, Niu X and El-Sheimy N 2008 Civilian vehicle navigation: required alignment of the inertial sensors for acceptable navigation accuracies *IEEE Trans. Veh. Technol.* **57** 3402–12
- [21] Seo J, Lee H K, Lee J G and Park C G 2006 Lever arm compensation for GPS/INS/odometer integrated system *Int. J. Control Autom. Syst.* **4** 247–54
- [22] Gao N and Zhao L 2016 An integrated land vehicle navigation system based on context awareness *GPS Solut.* **20** 509–24
- [23] Wang M, Wu W, He X, Li Y and Pan X 2019 Consistent ST-EKF for long distance land vehicle navigation based on SINS/OD integration *IEEE Trans. Veh. Technol.* **68** 10525–34
- [24] Singer R A and Sea R G 1971 Increasing the computational efficiency of discrete Kalman filters *IEEE Trans. Autom. Control* **16** 254–7
- [25] Dong Y, Wang D, Zhang L, Li Q and Wu J 2020 Tightly coupled GNSS/INS integration with robust sequential Kalman filter for accurate vehicular navigation *Sensors* **20** 561
- [26] Mu M and Zhao L 2019 A GNSS/INS-integrated system for an arbitrarily mounted land vehicle navigation device *GPS Solut.* **23** 112
- [27] Han S and Wang J 2012 Integrated GPS/INS navigation system with dual-rate Kalman filter *GPS Solut.* **16** 389–404
- [28] Nourmohammadi H and Keighobadi J 2018 Design and experimental evaluation of indirect centralized and direct decentralized integration scheme for low-cost INS/GNSS system *GPS Solut.* **22** 65